Journal of Ovonic Research Vol. 16, No. 5, September - October 2020, p. 293 -308

# IMPACT OF CHROMIUM DOPING ON STRUCTURAL, OPTICAL, MAGNETIC AND ELECTRICAL PROPERTIES OF NANO-COPPER FERRITE

S. A. GAD[a,*], A. M. MOUSTAFA[a], A. A. AZAB[b], A. F. HEGAB[a]
[a]*Solid State Physics Department, Physics Division, National Research Centre, 33 El Bohouth St. (former El Tahrir St.), Dokki, P.O. Box 12622, Giza, Egypt*
[b]*Solid State Electronics Laboratory, Solid State Physics Department, Physical Research Division, National Research Centre, 33 El-Bohouth St., Dokki, Giza 12622, Egypt*

Nanoparticles copper ferrites doped with chromium $CuCr_xFe_{2-x}O_4$ ($0 \leq x \leq 0.25$) were prepared using sol-gel auto combustion. Analysis of XRD revealed that the samples crystallized in single phase tetragonal $CuFe_2O_4$ structure. Results of Rietveld refinement using Full proff program showed that the lattice parameter a increased, lattice parameter c, the unit cell volume and tetragonal distortion decreased with increasing $Cr^{3+}$ concentration. A cation distribution ensured that a system ($CuCrFeO_4$) is completely inverse and distorted. In addition, crystallite size increased with the increase of $Cr^{3+}$content.Furthermore, optical energy band gap of the obtained spinel ferrite decreased from 2.441eV to 2.228 eV with the increase of Cr. Results of magnetic properties indicated that the saturation magnetization decreased from 24.1 to18.3 emu/g with Cr increment, due to a lower magnetic moment of $Cr^{3+}$ ion (3mB) than that of $Fe^{3+}$ ion (5mB).Coercivity decreases with increasing Cr-concentration can be attributed to the reduction in magnetocrystalline anisotropy (K) where, chromium ferrite has negative magnetocrystalline anisotropy. Squareness ratio decreased continuously with Cr content, which it displayed that the materials exhibited to soft magnetic properties. Dielectric properties were analyzed in frequency range (0.1-7MHz) at different temperatures (50-150°C).From electrical measurements, it was found that ε decreased at lower frequency, become nearly constant at higher frequencies for all samples and increased with increasing temperature. ε was found to increase with increasing Cr because the Cr is reducing the hopping probabilities across the grain boundaries. . Also, it was found that activation energy ΔE decreased with increasing Cr concentration.

(Received August 5, 2020; Accepted October 12, 2020)

*Keywords:* $CuCr_xFe_{2-x}O_4$ nanoparticles,Spinel ferrites, Structural analysis, Optical properties, Magnetic properties, Dielectric properties

## 1. Introduction

Spinel ferrites based on copper and iron oxides $CuFe_2O_4$ have many applications such as magnetic recording media, electronic devices and medical applications like as drug delivery systems and cancer therapy [1–3]. $CuFe_2O_4$ is a p-type semiconductor and its optical energy band gap ≈1.4eV so; it is suitable for solar photocatalytic applications like solar water splitting. Because of these materials have high (electrical resistivity, permeability), negligible eddy current losses, magneto-resistive and magneto-optical properties; it can be used in a broad range of power applications [4]. This material is interesting because it crystallizes either in a tetragonal or cubic symmetry depending on a cation distribution among the interstitial sites of its spinel structure [5, 6].

Different techniques have been used for synthesizing of ferrite materials including co-precipitation, combustion, hydrothermal/solvothermal, microwave synthesis, sol–gel method, and sol gel auto combustion [7-12]. Ferrites nanomaterials are of great importance because of its optical, electrical and magnetic properties, which makes it useful materials for various scientific and industrial applications such as flexible recording media, superconductors, and magnetic refrigerator [13]. On the other hand, there several factors affect on electrical and dielectric

* Corresponding author: samiagad2000@yahoo.com

properties of ferrites such as preparation technique, sintering (temperature, atmosphere& time) and chemical composition [14-17]. Moreover, it is interesting to investigate electrical and dielectric properties of nano-crystalline copper and substituted copper ferrite. Minor changes in size and surface effects of ferrites make it possible to have unique magnetic properties. First aim of the present work is preparing mixed spinel ferrite nano-powder $CuCr_xFe_{2-x}O_4$($x$ = 0, 0.05, 0.1, 0.15, 0.2 and 0.25) by alittle cost and effective method auto combustion and investigating effects of mixing parameter (x) on both structure and microstructure properties. Secondly, is studying physical properties (optical, dielectric and magnetic) and correlate these properties with structural parameters.

## 2. Experimental and preparation

$CuCr_xFe_{2-x}O_4$($x$ = 0, 0.05, 0.1, 0.15, 0.2 and 0.25) prepared by sol-gel auto combustion method. Calculated amounts of stoichiometric required metal nitrates were dissolved together in a 100ml of deionised distilled water to get clear solution. Nitrates were taken in certain stoichiometric ratio in a glass beaker and heated at 80°C on a hot plate for about 10 minutes with constant stirring by using cleaned glass rod. After that, a solution of citric acid with appropriate proportion added to nitrate solution. In order to adjust the pH value to about 7, a required amount of ammonia is added into the solution. The process of mixing continued and the mixture was heated at 400°C till burning the material in powder form. Finally, the powder was annealed in alumina crucibles in air at 750°C for 6hrs. X-ray diffraction (XRD) of investigated compounds were recorded at 300 K using an Emprean PANalytical X-ray diffractometer equipped with filtered CuKa radiation (λ=1.5406Å) using a step-scanning mode, in the angular range 15–80° 2θ, the step size 0.02° 2θ and step time 20 s/step. Diffuse reflectance was determined in the range 200- 2000 nm using a double beam spectrophotometer; JASCO V-570 model. Vibrating sample magnetometer model 9600-1-VSM was used for the magnetic properties measurements. Dielectric measurements were carried out in frequency range 0.1Hz – 20MHz and at a temperature range from 30 to 150ºC using a Novocontrol high resolution alpha analyzer.

## 3. Results and discussion

### 3.1. SEM

Scanning Electron Microscope is a technique used to find out the morphology (shape of nanoparticles) of the samples. Figs. (1a, b, c & d) represent SEM and EDAX of $CuFe_2O_4$ and $CuCr_{0.1}Fe_{1.9}O_4$ samples calcined at 750°C. From these figures we observe that an agglomeration of particles due to the interaction between magnetic nanoparticles and the heat generated during the preparation process. EDX of samples confirms the presence of consisting elements as follows Cu, Cr, Fe and O, and ensures that they are nearly stoichiometric.

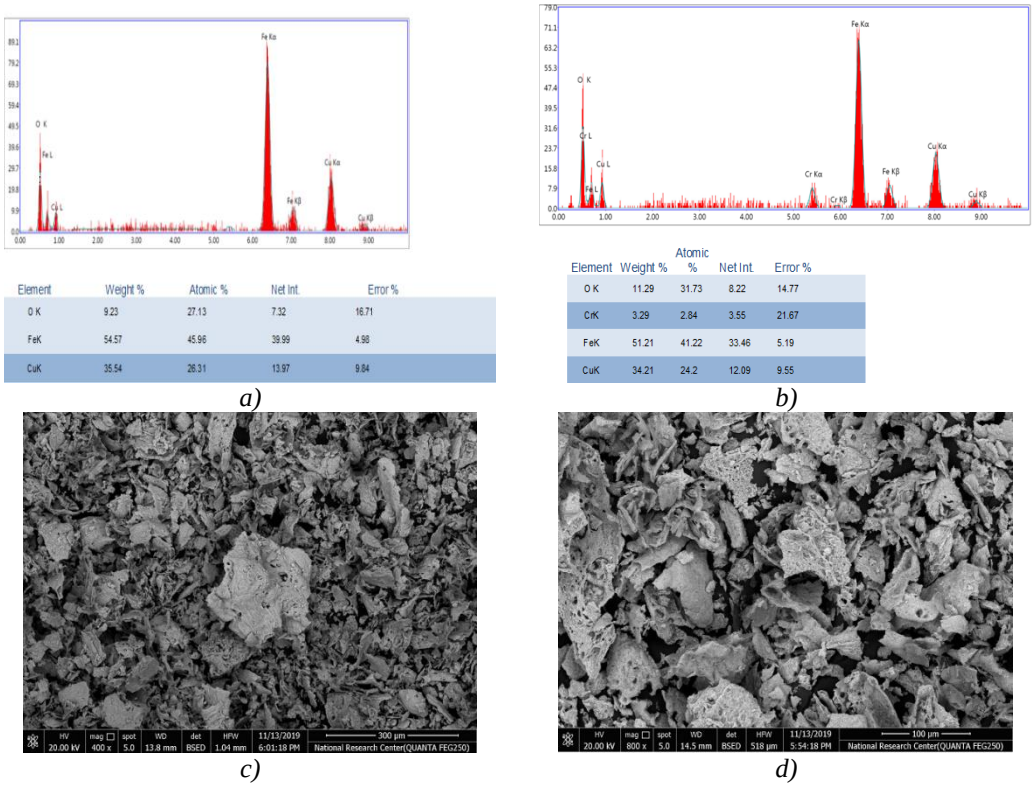


*Fig. 1.(a) EDAX of $CuFe_2O_4$, (b) EDAX of $CuCr_{0.1}Fe_{1.9}O_4$, (c) SEM image of $CuFe_2O_4$, (d) SEM image of$CuCr_{0.1}Fe_{1.9}O_4$.*

### 3.2. Structural

From the closer look to the obtained diffraction pattern shown in Fig. 1,it is clear that $CuCr_xFe_{2-x}O_4(0.0\leq x\leq 0.25)$ calcined at 750°C crystallized in nanostructure due to the broadened of diffraction peaks. All detectable peaks are indexed as tetragonal $CuFe_2O_4$ with an inverse spinel structure, as shown in standard data (PDF: 340425) with no impurity peaks corresponding to any other phase. Same behavior has been obtained with A. S. Padampalle et al. [18-20]. In general, the crystal structure of $CuFe_2O_4$ can be either cubic or tetragonal depending on the concentration of Cu ions occupying octahedral sites and the preparation method. D. Thapa et al [21] report same symmetry of copper ferrite.

Various tetrahedral (A) and octahedral (B) sites distributions can be obtained by the addition of metal cations of different valence states in spinel ferrites [22]. As many important properties of ferrites depend on the nature of cation distribution over the octahedral and tetrahedral sites in spinel lattice [23, 24], then any change in distribution of cations among tetrahedral and octahedral site have very dominant effects on the physical properties [25]. Chromium substitution in copper ferrite could produce sufficient changes in spinel structure and the substitution of $Cr^{3+}$ ions have a strong B-site preference for $Fe^{3+}$ ions that will alter magnetic properties [26]. A. M. Moustafa et al studied the cation distribution and magnetic properties of nickel doped copper chromium ferrite and they found that the degree of inversion depends on nickel concentration and they concluded that cation distribution is the major part in deciding the final magnetic properties of ferrite [27]. Therefore, a precise knowledge of the cations distribution among the available crystallographic sites of the spinel lattice is essential to understand the various physical properties of ferrites. So, a Rietveled refinement [28] was conducted on all samples using Full Proff Program [29].

To model the peak profile of the patterns based on body sintered tetragonal I41/amd space group in which the cations located at the tetrahedral sites at 8c Wyckoff position (0, ¾, 0.125) and that located at octahedral sites at 4b (0,0,0,5) while the oxygen anions occupy the Wychoff position 16h (0, 0.016, 0.25). The instrumental constants were determined using standard annealed

Quartz sample. To determine the cation distribution, we assumed that $Cr^{3+}$ ions occupy its preferential octahedral sites; based on its favorable charge distribution in the crystal field of octahedral site [30, 31], and $Fe^{3+}$ and $Cu^{2+}$ ions are distributed among the two lattice sites. In addition to the occupancy of the same ion in two lattice sites connected with the same code and lets it refined freely.

The structural and microstructural parameters obtained from Rietveld analysis are given in Table 1. The $\chi 2$ values (1.2 - 1.4) suggest good refinement of data as seen in Fig. 2. From this table, it is clear, that the preference of $Cu^{2+}$ and $Cr^{3+}$ cations to occupy octahedral sites and$Fe^{3+}$ cations to relocate and fully occupy tetrahedral sites beside octahedral sites at spinel structure i.e. chromium doped copper ferrite crystallized in completely inverse spinel structure. These results are in agreement with that obtained by Ata-Allah on Mössbauer data [32] of copper ferrite, and similar results, were obtained by Balagurov*et. al.*[33].

*Table 1. Refined Values of lattice parameters, unit cell volume, crystallite size, discrepancy factors Goodness of fit index $\chi 2$, bond lengths and bond angles for the compounds $CuCr_xFe_{2-x}O_4$ ($0 \leq x \leq 0.25$).*

| x | 0.0 | 0.05 | 0.1 | 0.15 | 0.2 | 0.25 |
|---|---|---|---|---|---|---|
| a | 5.81367(7) | 5.8137 | 5.8141(2) | 5.8193(1) | 5.8225 (1) | 5.8328(1) |
| c | 8.6917(2) | 8.6916 | 8.6843(3) | 8.6675(2) | 8.6460(2) | 8.6034(3) |
| c/a | 1.4950 | 1.495 | 1.4937 | 1.4894 | 1.4849 | 1.475 |
| Y(o) | 0.0206(7) | 0.0205(8) | 0.0189(7) | 0.0154(8) | 0.0114(6) | 0.0090(7) |
| Z(O) | 0.2536(5) | 0.2535(5) | 0.2566(5) | 0.2594(5) | 0.2575(4) | 0.2601(5) |
| Volume $Å^3$ | 293.77(1) | 293.77 | 293.56(2) | 293.52(1) | 293.11(1) | 292.7(2) |
| Crystallite Size nm | 14 | 17 | 18 | 17 | 23 | 25 |
| $R_p$ | 70.8 | 70.5 | 66.4 | 70.6 | 59.8 | 63.5 |
| $R_{wp}$ | 35.4 | 35.4 | 34.5 | 36.5 | 32.9 | 35.4 |
| $R_{exp}$ | 29.6 | 29.5 | 30.8 | 33.9 | 30.5 | 29.91 |
| $\chi^2$ | 1.43 | 1.44 | 1.25 | 1.16 | 1.167 | 1.4 |
| O-Cu x 2 | 2.145(4) | 2.146(4) | 2.117(4) | 2.087(4) | 2.098(4) | 2.065(5) |
| O-Cu x 4 | 1.973(3) | 1.973(3) | 1.980(3) | 1.997(3) | 2.013(2) | 2.027(3) |
| Cu-Fe | 2.9911 | 2.9911 | 2.9898(1) | 2.9880 | 2.9849 | 2.9797(1) |
| Cu-Fe | 2.9068 | 2.9069 | 2.9070(1) | 2.9087(1) | 2.9112 | 2.9164 |
| Fe-O | 1.930(4) | 1.929(5) | 1.937(4) | 1.935(5) | 1.905(3) | 1.906(5) |
| O-Fe-O (Tet.) | 109.2(2) | 109.6(1) | 110.4(1) | 111.3(1) | 111.2(1) | 111.8(2) |

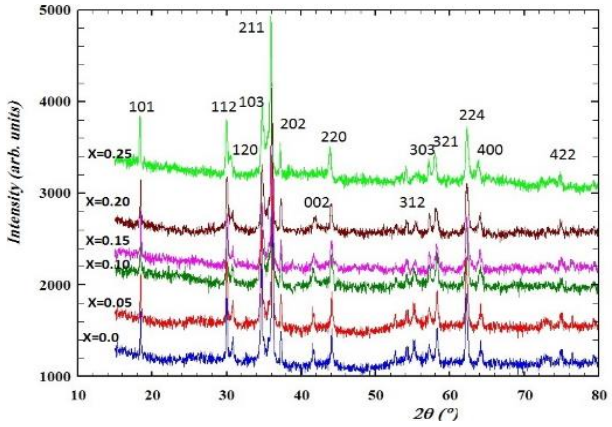


*Fig. 2. X-Ray diffractogram of a series of $CuFe_{2-x}Cr_xO_4$, $0.0 \leq x \leq 0.25$.*

As shown in Table 1 the lattice parameter a increases and the lattice parameter c decreases with composition parameter x. This may be due to cation replacement; the $Cu^{2+}$ ions replacing $Fe^{3+}$ions in B-sites. This behavior of lattice constant is an indication that the system ($CuCrFeO_4$) under investigation is completely inverse and distorted. Also, it will be noticed from refined values of unit cell volume tabulated in Table 1 that, unit cell volume decreases with increasing the $Cr^{3+}$ content this may be due to the difference in ionic radius between $Cr^{3+}$= 0.755Å and $Fe^{3+}$= 0.785Å. [34].

Tetragonal distortion is the most common distortion in spinel structure, this distortion is explained by Jahn- Teller theory according to it, a non-linear molecule in ground state is unstable in the symmetric configuration, and it will distort itself to lower its energy. The ions with $3d^4$ or $3d^9$ electronic configuration, when situated at the octahedral site cause a strong tetragonal distortion (c/a >1). Whereby one of the cubic axes would elongated with respect to the other two. As a result of oxygen octahedra around the B, sites are elongated parallel to the c axis with two longer B-O distance = 2.145(4) Å, and contracted in the ab plane with 4 B-O distance = 1.973(3) Å for x=0.0, see Table 1. If no additional symmetry breaking occurs, the tetragonal distortion alone decreases the symmetry from Fd3m (Z=8) to I41/amd (Z=4, see Fig. 2). From Table 1 it can be noted that, the axial ratio (c/a) for $CuFe_{2-x}Cr_xO_4$ (x = 0.0) is found to be 1.4950 and it decreases to 1.4750 for x = 0.25 composition, suggests that, decreasing of tetragonal distortion with increasing Cr- content (x). In spinel structure, each of the four vertices of tetrahedron is shared with vertices of octahedra aligned parallel to the c-axis direction as shown in Fig.3. The modification of the octahedral geometry along the c-axis direction, therefore, interacts directly with the compression or elongation of the tetrahedral geometry along the c-axis direction. As a result of that, the tetrahedral bond angle O-T-O increases from 109.6°(2) to 111.8(2). Finally, values of the crystallite size tabulated in Table 1 indicated, that the crystallite size tends to increase with increasing $Cr^{3+}$content; because of Cr cation leads to coalescence of the crystallites that result in increasing the average size of particles [35].

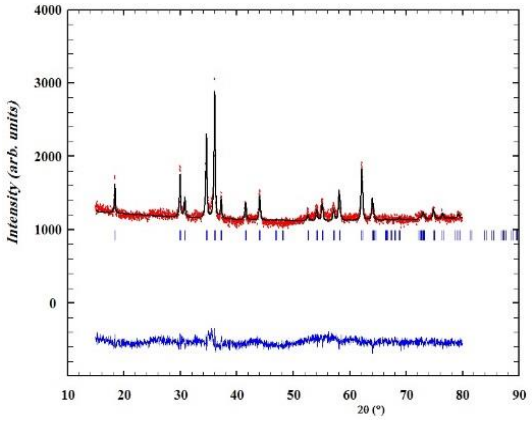


*Fig. 3. Final Rietveled refinement for $CuFe_{1.9}Cr_{0.1}O_4$, observed (closed circles),calculated (solid line) X-ray diffraction profiles and the difference between them (on the bottom). Vertical bars refer to calculated Bragg peak positions.*

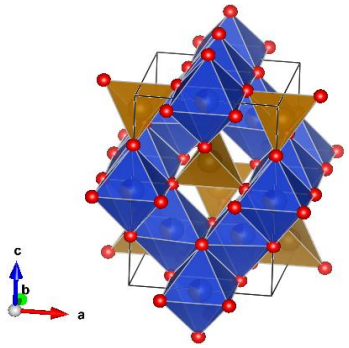


*Fig. 4. Geometrical representation of cubic spinel structure, view along b axis.*

## 4. Optical properties

Optical energy band gap ($E_g$) of $CuCr_xFe_{2-x}O_4$ ($x$ = 0, 0.05, 0.1, 0.15, 0.2 and 0.25) was studied by means of diffuse reflectance. Fig.5 illustrates a relation between diffuse reflectance (DR %) and wavelength (λ) in range (200-2000nm).

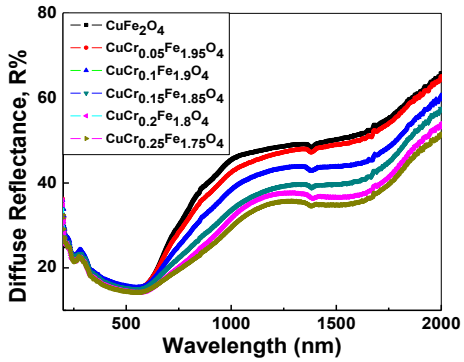


*Fig. 5. Relation between diffuse reflectance and wavelength (λ) for$CuFe_{2-x}Cr_xO_4$(0.0≤x≤0.25).*

It is found that at about 1000 nm, a decrease in reflectance is observed due to fundamental absorption (valance band to conduction band) by a material [36]. The more universal method of determining a position of absorption edge is the onset of this drop [37]. Energy gap can be obtained from the linear increase in diffuse reflectance as a function of wavelength. Also, Kubelka-Munk equation is used to analyze DR% spectra [38]. *F(R)* was derived by using Kubelka -Munk, has proportionality with absorption coefficient (α):

$$F(R) = \frac{(1-R)^2}{2R} = \frac{k}{S} \quad (1)$$

Where *R*, *k* and *s* are absolute reflectance, absorption and scattering coefficients of the samples respectively. A dependence of $E_g$ on $\alpha$ is known as Tauc relation [39-41]. Moreover, David and Mott indicated that optical absorption depends on $h\upsilon$ and $E_g$ as following [42, 43]:

$$(\alpha h\nu) = B\,(h\nu - E_g)^n \quad (2)$$

Where h, ν, B are Planck constant, frequency, constant and n determines the nature of electronic transition. Fig.6 gives Tauc plots of $(\alpha h\upsilon)^2$ vs. $h\upsilon$ for all samples. On the other hand, Fig.7 represents a relation between direct allowed $E_g$ and Cr content.

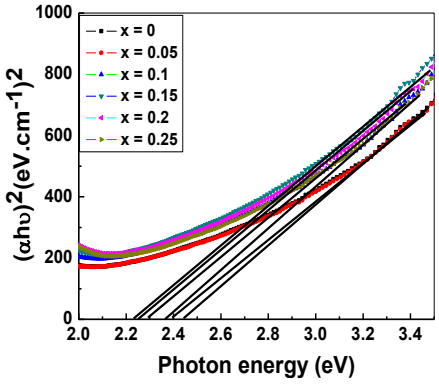


*Fig. 6. The dependence of $(\alpha h\nu)^2$ on photon energy ($h\nu$).*

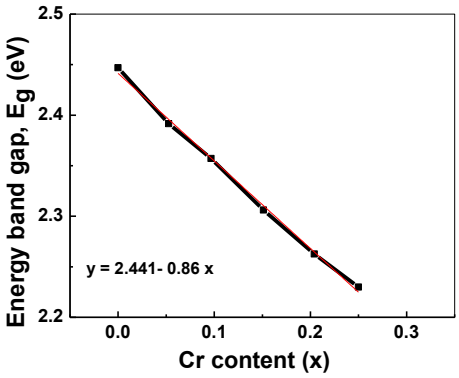


*Fig. 7. Variation of energy band gap ($E_g$) with Cr content.*

It is obvious that a decrease of $E_g$ with increasing Cr ratio. This decrement in $E_g$ may be due to the differences in particle size, according to Brus model [44]:

$$\Delta E_g \sim \left(\frac{h^2\pi^2}{2r^2\mu}\right) - \left(\frac{1.876e^2}{\varepsilon r}\right) + \cdots (3)$$

Where $\mu$, e, r and $\varepsilon$ are effective carrier mass, electron charge, particle size and static dielectric constant respectively. Also, a decrease may be due to ionic radii of $Cr^{+3}$ (0.755 Å) is smaller as compared to $Fe^{+3}$ (0.785Å). In addition, a variation of $E_g$ with $x$ (*Cr* content) can be fitted to a linearly form as shown in Fig.7, $E_g$= 2.441- 0.86 x, where 2.441eV is transition energy of a sample with $x$ = 0.

## 5. Magnetic properties

Fig.8 demonstrates magnetization variation versus magnetic field strength and Cr content $CuCr_xFe_{2-x}O_4$. Hysteresis loop curves give information about magnetic behavior and magnetic parameters of samples and such as saturation magnetization (*Ms*), coercivity (*Hc*), remanent magnetization (*Mr*) and squareness ratio (*Mr/Ms*). These parameters which obtained from hysteresis loop were tabulated in Table 2. Dependence of *Ms* and *Hc* on Cr substitution content in $CuCr_xFe_{2-x}O_4$is seen in Fig.9.From this figure, it is clear that, *Ms* decreased from 24.1 to18.3 emu/g with increasing of Cr content [35, 45]. Decrement in values of *Ms* with $Cr^{3+}$ ions content can be interpreted according to theory of Neel's two sub-lattice model of ferrimagnetisms [46-48]. For ferrites, a net magnetization resulted from the uncompensated electron spin and spin alignments of an individual ions in octahedral B-sites which it anti-parallel to those in tetrahedral

A-sites[49,50].According to Neel's model, A–B super-exchange interactions prevail B–B and A–A exchange interactions[51].Where $Cr^{3+}$ ions preferentially occupy octahedral B sites[52],so, substitution of highly magnetic moment $Fe^{3+}$ (5 μB) located in octahedral sites by lower magnetic moment $Cr^{3+}$ (3 μB) ions resulting a decreasing in net magnetization as well as the exchange interactions of sublattices. Fig. 9 shows that, *Hc* decreased from 1010 Oe to 474 Oe with increasing Cr content up to x = 0.25. Coercivity is affected by many parameters such as magnetocrystallinity, particle shape morphology, microstrain, and size distribution [50]. Decrement in magnetic coercivity values with Cr-concentration can be referred to decrease in magnetocrystalline anisotropy (K) where, chromium ferrite has negative magnetocrystalline anisotropy [54]. The lower values of coercive field with Cr content improve soft ferromagnetic properties, and enhance their uses in high-frequency transformers applications. From Table 2squareness ratio decreases continuously with Cr content, which it paves way to achieve soft magnetic properties.

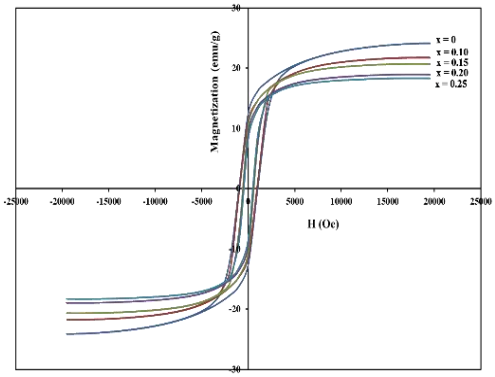


*Fig. 8. Hysteresis loop of $CuFe_{2-x}Cr_xO_4$ ($0.0 \leq x \leq 0.25$) nanoparticles.*

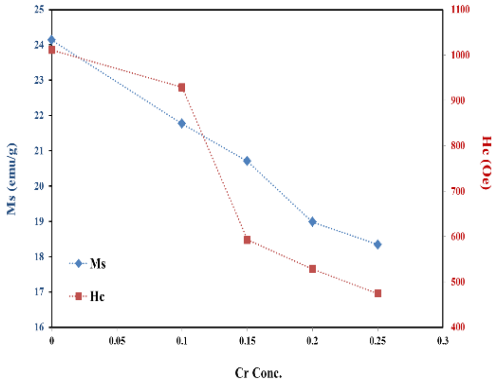


*Fig. 9. Saturation magnetization (Ms) and coercivity (Hc)vs. Cr concentration.*

*Table 2. Magnetic parameters (saturation magnetization (Ms), remnant magnetization (Mr), coercivity (Hc) and squareness ratio (Mr/Ms) at room temperature for $CuCr_xFe_{2-x}O_4$ ($0 \leq x \leq 0.25$).*

| X | Ms (emu/g) | Mr (emu/g) | Hc (Oe) | R (Mr/Ms) |
|---|---|---|---|---|
| 0.00 | 24.1 | 12.4 | 1010 | 0.52 |
| 0.10 | 21.8 | 11.3 | 929 | 0.51 |
| 0.15 | 20.7 | 10.4 | 592 | 0.50 |
| 0.20 | 18.9 | 9.1 | 531 | 0.48 |
| 0.25 | 18.3 | 8.1 | 474 | 0.44 |

## 6. Dielectric properties

Measurements of a real part of dielectric constant (έ) and dielectric loss (ε̋) were carried out in frequency (ν) range (0.1 -7 MHz) at different temperatures (50-150°C). From Fig. 10 (a, b, & c) it is clearly shown that, έ decreases steeply at lower frequency and become nearly constant values for all samples at higher frequencies and increases with increasing temperature which are in agreement with spinel ferrites [55,56].

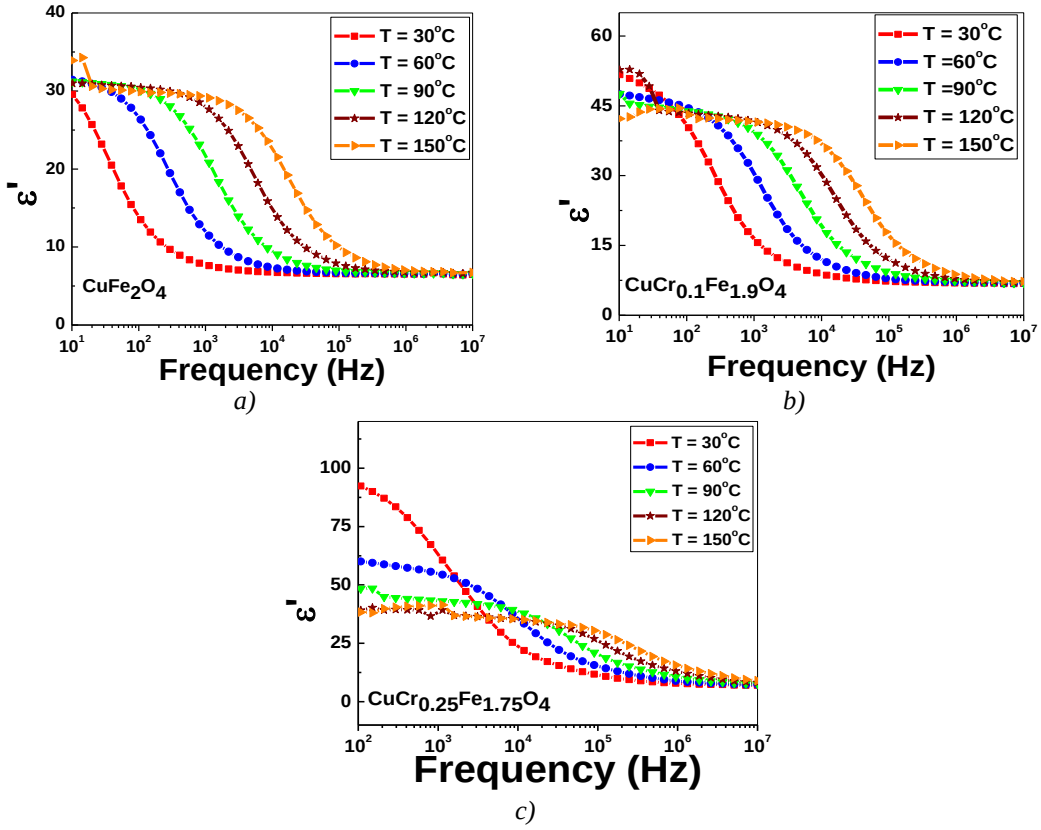


*Fig. 10. a) Dependence of dielectric constant (έ) on frequency of $CuFe_2O_4$, b)Dependence of dielectric constant (έ) on frequency of$CuCr_{0.1}Fe_{1.9}O_4$, c) Dependence of dielectric constant (έ) on frequency of $CuCr_{0.25}Fe_{1.75}O_4$.*

Same behavior can be obtained for ε̋ as shown in Fig.11 (a, b & c). Decrement in έ at low frequency indicates dielectric dispersion. This dispersion in dielectric behavior is due to Maxwell–Wagner type interfacial polarization in accordance with Koop's phenomenological theory [57]. Based on this theory the dielectric structure is composed of two layers, one is fairly well conducting grains, which is separated by a thin layer of poorly conducting substances, which forms the grain boundary. Charge carriers reach the grain boundary via hopping at lowν, and charge carriers pile up at grain boundaries and produce polarization if the resistance of the grain boundary is high enough. However, as the frequency of applied field is increased beyond a certain value, the charge carriers hopping cannot follow the alternating field fluctuations and as a result, polarization decreases. So, έ decreases as νincreases of the applied field. Same behavior was observed in many spinel ferrites [55,56].

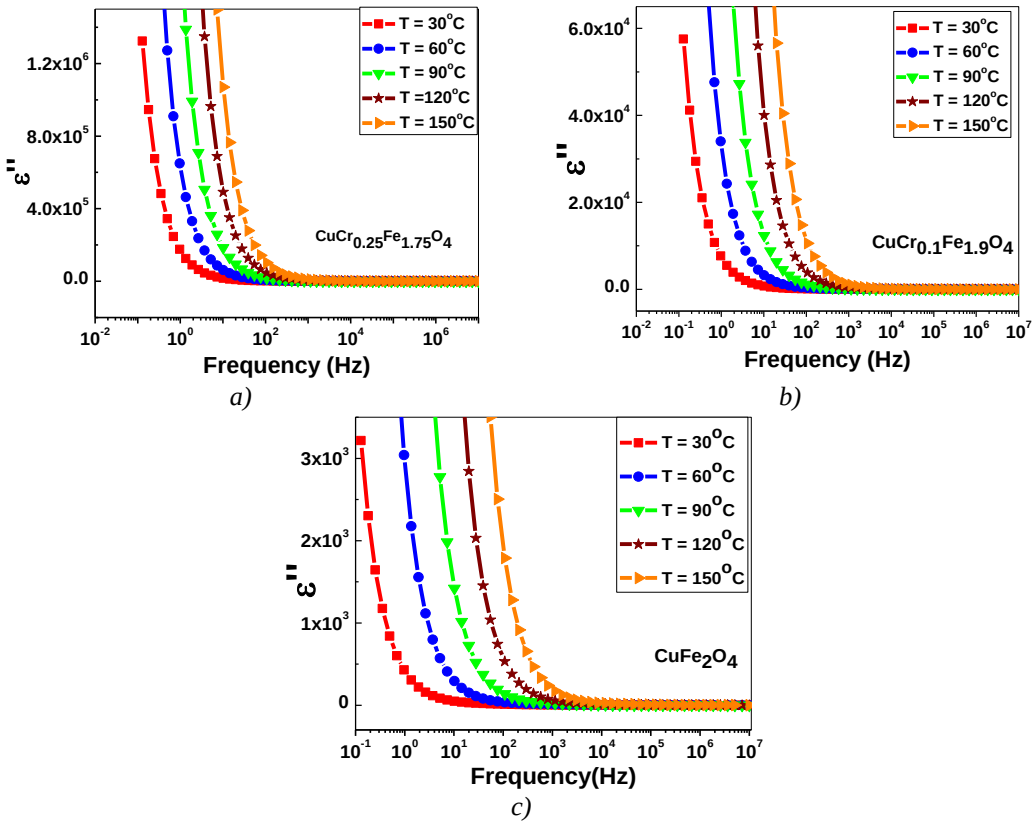


*Fig. 11. Dependence of dielectric loss(ε̋) on frequency of $CuFe_2O_4$, b)Dependence of dielectric loss(ε̋) on frequency of $CuCr_{0.1}Fe_{1.9}O_4$, c) Dependence of dielectric loss(ε̋) on frequency of $CuCr_{0.25}Fe_{1.75}O_4$.*

Fig. 12 represents a relation between ε' and Cr content, from this figure it is clear that έ increases with increasing Cr which is in good agreement with an earlier report [58]. A reason for this variation may be due to Cr concentration, which is reducing the hopping probabilities across grain boundaries. This causes increasing the charge accumulation at grain boundaries and hence έ value. Same behavior has been obtained by Ali M. Mohammad et al. [59].

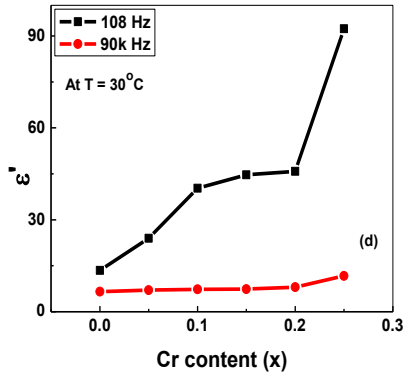


*Fig. 12. Variation of dielectric constant (έ) with Cr content at 108Hz and 90 kHz.*

Electric modulus formalism ($M^*$) has been studied, to remove high loss effects, especially at low frequencies. When an electric displacement remains constant, electric modulus coincides to a relaxation of electric field in materials. $M^*$ can be calculated by using this equation:

$$M^*(\omega) = \frac{1}{\varepsilon^*(\omega)} = M'(\omega) + iM'' = \frac{\varepsilon'}{\varepsilon'^2+\varepsilon^{n2}} + i\frac{\varepsilon''}{\varepsilon'^2+\varepsilon^{n2}} \quad (4)$$

Where $M'$ , $M''$and $\varepsilon^*$are real, imaginary parts of electric modulus and dielectric constant. Fig. 13(a, b & c) show $M''$ as a function of ν at different measured temperatures, from this curve it is seen that $M''$ increases with increasing ν, exhibits a maximum at $M''_{max}$. It is characterized by well resolved peaks at unique νat temperatures (30-150°C); the positions have been shifted toward higher νside with increasing of temperature and Cr content. A range in which charge carriers are mobile over long distances is determined by frequency region below the peak maximum ($M_{max}$). At frequency above peak maximum, the carriers are confined to potential wells, being mobile for short distances [60, 61]. A shift of peaks with Cr increment may be attributed to increasing of conductivity. Maximum frequency ($f_{max}$) values were obtained from $M''$peak. A relation between log$f_m$ and 1000/T is shown in Fig.14a; $f_m$ obeys Arrhenius equation as follows:

$$f = f_\circ \exp(\frac{-E_a}{kT}) \quad (5)$$

Where $_a$, $f_\circ$, k and $T$ are activation energy, pre-exponential factor, Boltzmann constant and absolute temperature respectively. Activation energy (ΔE) is estimated from the slope of Fig. 14a. From Fig. 14 b, it is noted that ΔE decreased with increasing Cr concentration.

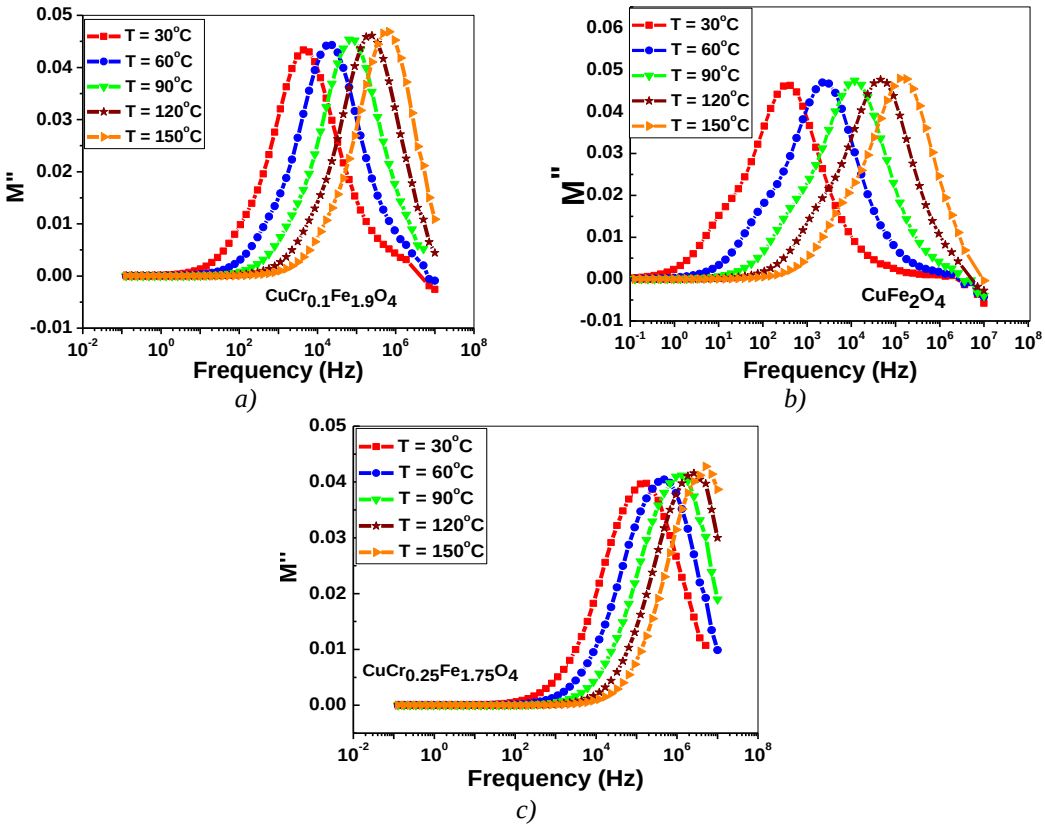


*Fig. 13. a)the relation between imaginary part of electric modulus (M'') and frequency of $CuFe_2O_4$. b) Relation between (M'') and frequency of $CuCr_{0.1}Fe_{1.9}O_4$. c) Relation between (M'')and frequency of $CuCr_{0.25}Fe_{1.75}O_4$.*

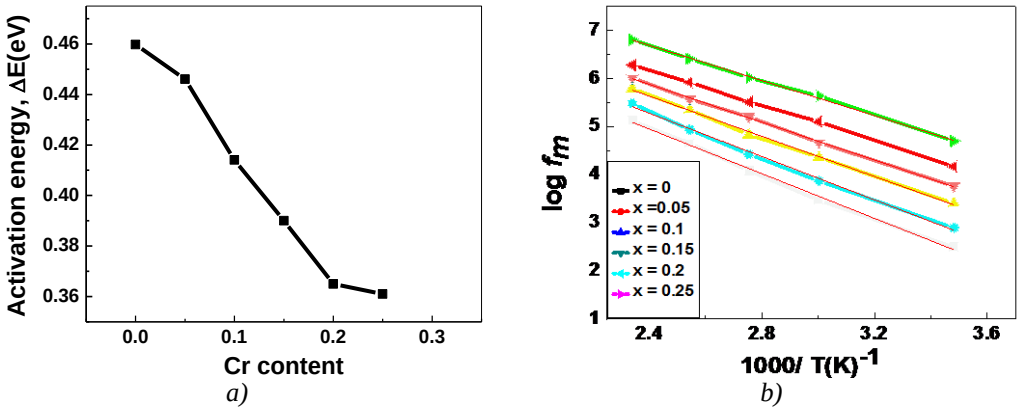


*Fig. 14.(a) The variation of log maximum frequency ($f_m$) vs. 1000/T, (b) Activation energy (ΔE) vs. Cr content.*

### 6.1. AC conductivity

Conductivity dependent on frequency is estimated from dielectric data by an equation [62, 63]:

$$\sigma_{ac} = \epsilon_o \epsilon_r \, \omega \tan \delta \quad (6)$$

where$\epsilon_o$ is permittivity of free space ($8.85 \times 10^{-14}$ F/cm), $\epsilon_r$ is relative permittivity, ω is angular frequency and tan δ is dielectric loss. Variation of $\sigma_{ac}$ with temperature supports thermally activated transport properties of material and obeys Arrhenius equation,

$$\sigma_{ac} = \sigma_{\circ} \exp(-E_a/kT) \quad (7)$$

where σ◦ is pre-exponential factor, $E_a$ is activation energy, k is Boltzmann constant and T is absolute temperature. Relation between AC conductivity ($\sigma_{ac}$) andν at different temperatures is seen in Fig. 15 (a, b &c), from this figure it is distinctly shown, that ($\sigma_{ac}$) increases with increasing temperature, which reveals semiconducting behavior of the samples. Frequency-independent behavior of conductivity in low-frequency region becomes sensitive in high-frequency region. Hopping frequency shifts towards higher frequency side at increasing temperature. Increment in frequency of applied field accelerates hopping of charge carriers results an increase in overall conduction process, thereby increasing $\sigma_{ac}$. Dependence of $\sigma_{ac}$on νclarifies dispersion in entire range of temperature i.e. replacing Cr instead of Fe in $CuFe_{2-x}Cr_xO_4$ compound affects the behavior of $\sigma_{ac}$with temperature and frequency. Moreover, conductivity increases with increasing temperature due to the increase in thermally activated drift mobility of charge carriers according to hopping conduction mechanism. $\sigma_{ac}$changes with a cation distribution in ferrites. Splitting of cation 3*d*-level into more stable triply degenerate *t*2g level (*d*xy, *d*yz, *d*zx atomic orbitals directed away from neighboring anions) can be produced from electrostatic interactions between anion and cation electrons and the less stable, doubly degenerate *e*g level (*d*z2, *d*x2−dy2 atomic orbitals directed towards neighboring anions) [64].

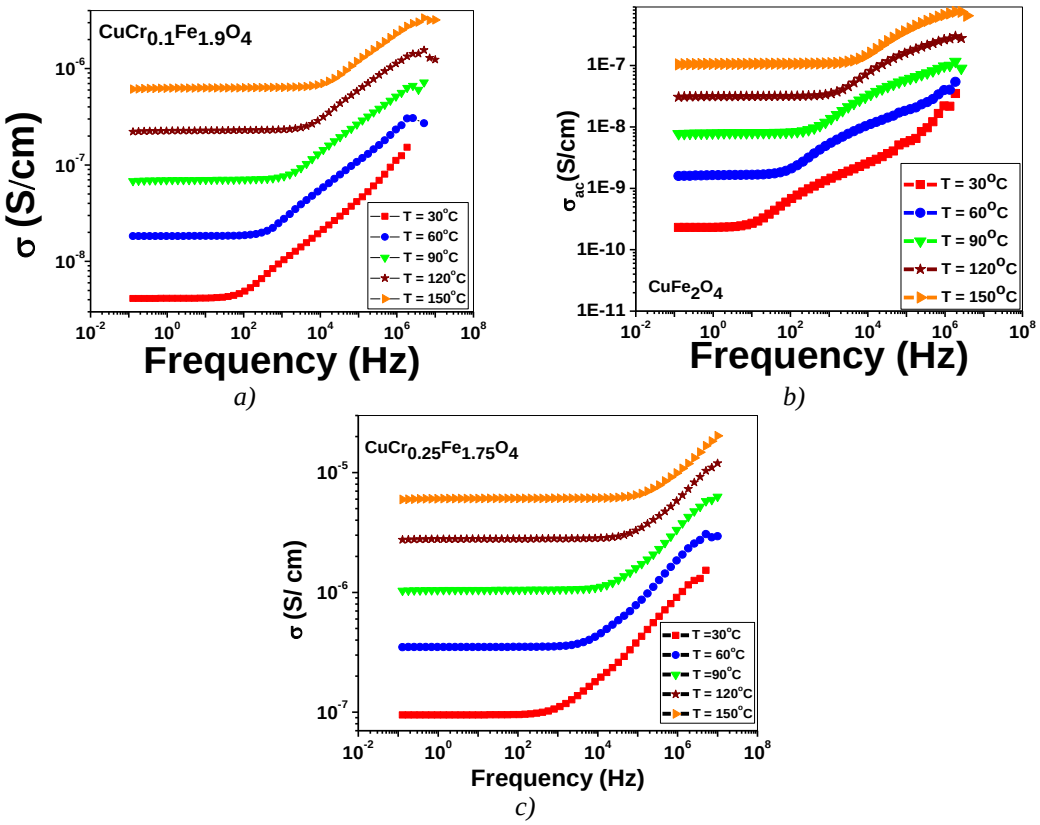


*Figs 15. (a) Relation between $\sigma_{ac}$ and ν at different temperatures of $CuFe_2O_4$ ;(b) Frequency dependence of $\sigma_{ac}$ at different temperatures of $CuCr_{0.1}Fe_{1.9}O_4$;(c) Frequency dependence of the $\sigma_{ac}$ at different temperatures of $CuCr_{0.25}Fe_{1.75}O_4$.*

*Table 3. The calculated values of s factor.*

| Temperature (°C) | x=0.0 | x=0.05 | x=0.10 | x=0.15 | x=0.20 | x=0.25 |
|---|---|---|---|---|---|---|
| 30 | 0.3538 | 0.3413 | 0.3348 | 0.3845 | 0.3734 | 0.3211 |
| 60 | 0.2997 | 0.3004 | 0.3101 | 0.367 | 0.3626 | 0.3118 |
| 90 | 0.262 | 0.2847 | 0.2885 | 0.3547 | 0.3578 | 0.3041 |
| 120 | 0.225 | 0.2777 | 0.2736 | 0.3382 | 0.3424 | 0.2908 |
| 150 | 0.1855 | 0.2904 | 0.2812 | 0.3246 | 0.3241 | 0.2792 |

Goodenough and others [65-68], reported that cation–anion–cation and cation–cation interactions can be presented in rocksalt–type structure and spinel structure. These materials have a metallic behavior and may become semiconductor at low temperature in case of strong cation–cation interactions between octahedral *B*-site cations. Charge transfer between octahedral cations by hopping of localized *d* electrons leads to transport properties. This hopping mechanism is referred to valence distribution of cations that occupy the octahedral site. In present materials, $Cu^{2+}$ions in $CuFe_2O_4$ unit cell, are occupying octahedral *B*-sites as confirmed from results of Rieteveld refinement see table 1and agrees with the reported earlier [69-72]. Calculated values of s factor are listed in Table 3, it is noticed that s values decrease with increasing temperature which confirm that a conduction mechanism in our samples referred to the hopping conduction. When $s < 1$, the hopping motion is more probable, but when $s > 1$,the re-orientational motion happens and ions are well-localized [73].

## Conclusions

$CuCr_xFe_{2-x}O_4$ nanoparticles are successfully prepared by sol-gel auto combustion method. X-ray analysis revealed the formation of tetragonal $CuFe_2O_4$ spinel ferrite systems. Rietveld refinement showed that, tetragonal distortion decreased with $Cr^{3+}$ content and the resulting cation distribution proved that the ferrite systems are completely inverse spinel structure. Energy band gap of the spinel ferrite decreased with the increase of Cr concentration. Coercivity(*Hc*) and saturation magnetization (*Ms*) decreased with increasing Cr content. Squareness ratio decreased continuously with Cr content, which it showed that the materials exhibited to soft magnetic properties.

Dielectric properties were examined in a frequency range from (0.1 to 7MHz). It was found that dielectric constant ($\acute{\varepsilon}$) and dielectric loss ($\acute{\varepsilon}$) decreased at lower frequency, become nearly constant for all samples at higher frequencies, and increased with increasing temperature. In addition, AC conductivity increased with increasing temperature.

## References


[1] L. R. Rad, I. Haririan, F. Divsar, Spectrochim. Acta A **136**, 423 (2015).
[2] J. Chomoucka, J.Drbohlavova, D. Huska, V. Adam, R. Kizek,J. Pharmacol. Res. **62**, 144 (2010).
[3] B. Baruwati, S. V. Manorama, Mater. Chem. Phys. **112**,631(2008).
[4] N. Bao, L. Shen, Y. Wang, P. Padhan, A. Gupta, J. Am. Chem. Soc. **129**,12374(2007).
[5] G. F. Goya, H. R. Rechenberg, J. Z. Jiang, J. Appl. Phys. **84**, 1101 (1998).
[6] S. Marup, J. Z. Jiang, F. Bodker, A. Harsewell,Euro. Phys. Lett. **56**,441 (2001).
[7] S. Akbar Hosseini, J. Mat. Sci. **28**, 1086 (2017).
[8] R. Talebi, J. Mat. Sci. **27**, 6313 (2016).
[9] M. Vosoughifar, J. Mat. Sci. **27**, 10449 (2016).
[10] L. T. Lum, N. T. Dung, L. D. Tung, C. T. Thanh, O. K. Quy, N. V. Chuc, S.Maenosono, N. T. K. Thanh, Nanoscale **7**, 19596 (2015).
[11] M. Hashemi, F. Mohandes, S. Ahmadian-Fard-Fini, A. Sobhani, N. Shabani-Armaki, M. Salavati-Niasari, J. Mat. Sci. **28**, 11682 (2017).
[12] S. V. Jadhav, K. M. Jinka, H. C. Bajaj, Catal. Today**198**, 98 (2012).
[13] NaokiIkenaga, Yousuku Ohgaito, Hiroaki Matsushima, Toshimitsu Suzuki,Fuel **83**, 661 (2004).
[14] Souad Ammar, Arnaud Helfel, J. Mater. Chem.**11**, 186 (2001).
[15] I. M. Hamada, J. Magn. Magn. Mater. **271**,318 (2004).
[16] B. P. Ladgoankar, C. B. Kolekar, P. N. Vasamberkar, A. S. Vaingankar, Ind. J. Eng. Matt. Sci.**7**, 419 (2000).
[17] A. R.Lamani, H. S. Jayanna, P. Parameswara, R. Somashekar, R. R.Ramachander, G. D. Prasanna, J. Alloy. Compd. **509**, 5692 (2011).
[18] A. S. Padampalle, A. D. Suryawanshi, V. M. Navarkhele, D. S. Birajdar, International Journal of Recent Technology and Engineering (IJRTE) **2**(4), 2277 (2013).
[19] J. Q. Qi, W. P. Chen, M. Lu, Y. Wang, H. Y. Tian, L. T. Li, H. L. W. Chan, Nanotechnology **16**,3098 (2005).
[20] J. Z. Jiang, G. F. Goya, H. R.Rechenberg, J. Phys. Condens. Matter **11**, 4063 (1999).
[21] D. Thapa, N. Kulkarni, S. N. Mishra, P. L. Paulose, P. Ayyub,J. Phys. D: Appl. Phys. **43**, 195004 (2010).
[22]I. Gul, W. Ahmed, A. Maqsood,Journal of Magnetism and Magnetic Materials**320**(3-4), 270 (2008).
[23] M. J. Iqbal, Z. Ahmad, T. Meydan, Y. Melikhov, Journal of Magnetism and Magnetic Materials **324**(23), 3986 (2012).
[24] M. Vadivel,R. R. Babu, K. Sethuraman, K. Ramamurthi, M. Arivanandhan, Journal of Magnetism and Magnetic Materials**362**, 122 (2014).
[25] R. Panda, R. Muduli, G. Jayarao, D. Sanyal, D. Behera, Journal of Alloys and Compounds

**669**, 19 (2016).
[26] B. Toksha, S. E. Shirsath, M. Mane, S. Patange, S. Jadhav, K. Jadhav, The Journal of Physical Chemistry C **115**(43), 20905 (2011).
[27] A. M. Moustafa, I. S. Ahmed Farag, M. H. Abdellatif, M. A. Ahmed,Journal of Materials Science: Materials in Electronics **30**, 20099 (2019).
[28] H. M. Rietveld, J. Appl. Crystallogr. **2**(2) 65 (1969).
[29]J. Rodrguez-Carvajal, An Introduction to The Program (Version July 2017).
[30] H. Ohnishi, T. Teranishi,J. Phys. Soc. Jpn.**16**, 35 (1961).
[31] S. M. Patange, E. Sagar. Shirsath, B. G. Toksha,S. S. Jadhav, S. J. Shukla,K. M. Jadhav, Appl. Phys. A **95**, 429 (2009).
[32] S. S. Ata-Allah, J. Solid State Chem. **177**, 4443 (2004).
[33] A. M. Balagurov, I. A. Bobrikov, V. Yu. Pomjakushin, D. V. Sheptyakov, V. Yu. Yushankhai, J.Magn. Magn. Materials **374**,591 (2015).
[34] R. D. Shanon,ActaCryst.A**32**,751 (1976).
[35] M. Raghasudha, D. Ravinder, P. Veerasomaiah,J. Nanostruc. in Chem.**3**, 63 (2013).
[36] T.He, J. Yao, J. Photochem. Photobiol. C**4**, 125 (2003).
[37] P. D. Fochs, Proc. Phys. Soc. B**69**, 70 (1956).
[38] S. P. Tandon, J. P. Gupta, Phys. Stat. Solid. **38**(1), 363 (1970).
[39] J. Tauc, R. Grigorovici, A. Vancu, Phys. Stat. Solidi**15**(2), 627(1966).
[40] A. Baykal, S. Esir, A. Demir, S. Güner, Ceram. Int. **41**(1) A, 231 (2015).
[41] A. Baykal, S. Güner, A. Demir, S. Esir, F. Genç, Ceram. Int. **40**(8) B, 13401(2014).
[42] E. A. Davis, N. F. Mott,Philos. Magazine **179**, 903 (1970).
[43] N. F. Mott, E. A. Davis, Electronic Processes in Non-crystalline Materials, second ed., Clarendon Press (Oxford and New York), 1979.
[44] L. E. Brus, J. Chem. Phys. **80**(9), 4403(1984).
[45] M. A. Gabal, S. Kosa, T. S. El Muttairi, Ceramics International **40**(1), 675(2014).
[46] Neel L., C.R. Acad, Sciences Paris, 230,375 (1950).
[47] M. H. Abdellatif, G. M. El-Komy, A. A. Azab, M. Salerno,J. of Magn. andMagn. Mater. **447**, 15(2018).
[48] M. H. Abdellatif, G. M. El-Komy, S. A. Azab,J. Magn. andMagn. Mater.**442**, 445 (2017).
[49] A. A. Azab, E. M. El-Menyawy,J. of Electron. Mater.**48**(5), 3229 (2019).
[50] M.Javed Iqbal, Z. Ahmad, Y. Melikhov, I. C. Nlebedim, J. Magn. andMagn. Mater. **324**, 1088 (2012).
[51] R. N. Singha, N. K. Singha, J. P. Singh, G. Balaji, N. S. Gajbhiye, Journal of Hydrogen Energy**31**,701 (2006).
[52] G. L. Sun, J. B. Li, J. J. Sun, X. Z. Yang, J. Magn. Magn. Mater. **281**,173 (2004).
[53] S. T. Alone, E. ShirsathSagar, R. H. Kadam, K. M. Jadhav, J. Alloy. and Comp. **509**, 5055 (2011).
[54] J.Azadmanjiri, Mater. Chem. and Phys. **109**,109 (2008).
[55] G. R. Kumar, K. V. Kumar, Y. C. Venudhar, IJMER **2**(2) 177 (2012).
[56] B. H. Devmunde, A. V. Raut, S. D. Birajdar, S. J. Shukla, D. R. Shengule, K. M. Jadhav, J. of Nanoparticles **2016**, 1 (2016).
[57] C. G.Koops, Phys. Rev. **83**(1), 121 (1951).
[58] V. Vinayak, P. P. Khirade, S. D. Birajdar, R. Alange, K. Jadhav, Journal of Superconductivity and Novel Magnetism**28**(11), 3351 (2015).
[59] M. Mohammad Ali, M. Ridha, Sabah M. Ali, H. Mubarak Tahseen, Journal of Applied Engineering Research **13**(8), 6026 (2018).
[60] C. Bharti, T. P. Sinha,Solid State Sci.**12**(4), 498(2010).
[61] Mohamed M. Bakr, H. Wang, H. Fuess, J. Phys. D: Appl. Phys. **43**(45), 455409 (2010).
[62] I. Bunget, M. Popescu, Physics of Solid Dielectrics" (EdituraStiinsificasiEnciclopedica, Bucharest, 1978.
[63] S. A. Gad, A. M. Moustafa, A. A. Ward, J. Inorg. Organomet. Polym. **25**, 1077(2015).
[64] P. W.Anderson,Phys. Rev. **79**(2), 350 (1950).
[65] J. B. Goodenough, Direct Cation- -Cation Interactions in Several Oxides. ibid. **6**, 1442 (1960).

[66] S. S. Ata-Allah, M. K. Fayek,J. Phys. Chem. Solids**61**, 1529 (2000).
[67] S. S Ata-Allah, Mater. Chem. Phys. **87**(2-3), 378 (2004).
[68]H. P. Kiug, L. E. Alexander, X-Ray Diffraction Procedures 2nd ed., Wiley, New York, 1974.
[69] T. Murase, K. Igarahi, J. Sawai, T. Nomura, ICF7, Bordeaux, France, B3, 3 (1996).
[70] S. S. Ata-Allah, M. K. Fayek,Hper. Inter. **128**,467 (2000).
[71]Xiao-Xio Tang, A. Manthiram, I. B. Goodenough, J. Solid Stat. Chem. **79**, 250(1989).
[72] M. K. Fayek, M. F. Mostafa, F. Sayedahamed, S. S. Ata-Allah, M. Kaiser, J. Magn. Magn. Mater. **210**, 189 (2000).
[73] S. Karthickprabhu, G. Hirankumar, A. Maheswaran et al., J. Electrost. **72**(3),181 (2014).